Cancer Immunology, Immunotherapy (2022) 71:1075–1091
https://doi.org/10.1007/s00262-021-03055-7

ORIGINAL ARTICLE

LncRNA MIR155HG induces M2 macrophage polarization and drug resistance of colorectal cancer cells by regulating ANXA2

Lin Zhou[1] · Jian Li[1] · Mingmei Liao[1] · Qi Zhang[1] · Mei Yang[2]

Received: 26 November 2020 / Accepted: 7 September 2021 / Published online: 25 September 2021

Abstract

Objective To investigate the effects of lncRNA MIR155HG and Annexin A2 (ANXA2) on colorectal cancer (CRC) and the mechanism of the MIR155HG/ANXA2 axis.

Methods The expressions of MIR155HG and ANXA2 in human CRC tissues were analyzed for association with pathological characteristics and prognosis of CRC patients. CRC cell lines (Caco2 and HT29) were used to study the effects of MIR155HG or ANXA2 knockdown on tumor cell behaviors and macrophage polarization as well as the effect of M2 polarization on oxaliplatin resistance of CRC cells. RNA immunoprecipitation, RNA pull-down and dual-luciferase reporter assays were applied to verify the targeting relationships among MIR155HG, miR-650 and ANXA2. Heterotopic xenograft models were established to verify the results of cell experiments.

Results MIR155HG and ANXA2 were highly expressed in CRC tissues/cells and of prognostic values for CRC patients. Knockdown of MIR155HG or ANXA2 suppressed M2 macrophage polarization, and proliferation, migration, invasion and oxaliplatin resistance of CRC cells. MIR155HG competed with ANXA2 for binding miR-650 and can also directly target ANXA2. Knockdown of MIR155HG or ANXA2 also inhibited M2 macrophage polarization and CRC progression in nude mice.

Conclusion This study highlighted that MIR155HG, by regulating the miR-650/ANXA2 axis, promotes CRC progression and enhances oxaliplatin resistance in CRC cells through M2 macrophage polarization.

Keywords LncRNA MIR155HG · Annexin A2 · M2 macrophage polarization · Oxaliplatin resistance · MiR-650 · Colorectal cancer

Introduction

Colorectal cancer (CRC) is one of the commonest and deadly malignancies worldwide. Over 140,000 individuals were estimated to be diagnosed with CRC in the USA in 2020, among which 53,200 would die from the disease with an increased trend in individuals aged younger than 50 [1]. The incidence and mortality of CRC vary considerably due to discrepancies in human development index, and an increasing trend of CRC seems to be implicated with the adoption of a more western lifestyle [2]. The major risk factor for CRC is age, and beyond that, a personal or family history of CRC can also add to the risk of CRC [3]. Onset of a CRC is generally attributed to accumulative genetic and epigenetic alterations. Sporadic CRC accounts for about 75% of all CRC cases, which occurs in people without genetic predisposition to CRC [4]. Chronic inflammation is a vital initiator of CRC and inflammation elicited by an established tumor may further aggravate the cancer [5]. Patients with inflammatory bowel disease (IBD), such as Crohn's disease or ulcerative colitis, are susceptible to CRC under a prolonged inflammatory response induced by IBD [6].

Macrophages are highly plastic cells which can phenotypically transform from one type into another in response to micro-environmental stimuli and signals [7]. M1 macrophages are activated in Toll-like receptor (TLR) and interferon-dominated inflammatory settings, usually related

✉ Mei Yang
yangmei2852@163.com

[1] Department of General Surgery, Xiangya Hospital, Central South University, Changsha 410008, Hunan, People's Republic of China

[2] Department of Geriatric Medicine, Xiangya Hospital, Central South University, No. 87, Xiangya Road, Kaifu District, Changsha 410008, Hunan, People's Republic of China

to immunity to bacteria and intracellular pathogens, while M2 macrophages are associated with Th2 responses [8]. M1 macrophages are characterized with high expression levels of pro-inflammatory cytokines such as interleukin (IL)-6, IL-1β, tumor necrosis factor (TNF)-α and inducible nitric oxide synthase (iNOS), while M2 macrophages are marked by high levels of IL-10 and Arginase-1, among others.

M1 inflammatory mediators are considerably generated to promote tumorigenesis at an early stage while tumor-associated macrophages (TAMs) in established tumors mostly exhibit M2 properties [9]. TAMs provide immunosuppressive microenvironment for tumor cells and further secrete molecular mediators to enhance tumor angiogenesis, metastasis and drug resistance [10]. M2 polarization has already been demonstrated to be tumor-promotive in CRC. For instance, gut microbiota-induced cathepsin K contributed to M2 polarization of TAMs and further promoted metastasis of CRC cells [11]. TAMs in CRC were polarized into M2 phenotype by miR-145 shipped via tumor cell-derived extracellular vesicles, which in turn promoted tumor progression [12]. Moreover, increasing evidence has suggested that M2 polarization of TAMs plays a role in mediating drug resistance of tumor cells such as in breast cancer [13] and gastric cancer [14].

Over the decades, accumulating attention has been put on the role of long non-coding RNAs (lncRNAs) in cancers. LncRNAs are a heterogeneous and less conserved group of transcripts longer than 200 nucleotides and without protein-coding potential [15]. Broadly, lncRNAs can be categorized into sense, antisense, bidirectional, intronic and intergenic lncRNAs according to their location on the genome [16]. LncRNAs regulate gene expression primarily through interaction with other molecules at single or multiple regulatory levels including epigenetic, transcriptional, post-transcriptional, translational, and post-translational levels [17]. Dysregulation of lncRNAs such as XIST, RAMS11 and H19 is evidenced in CRC and those aberrantly expressed lncRNAs are often associated with tumor metastasis and malignant activities of cancer cells [18–20].

MIR155 host gene (MIR155HG), a novel member of the lncRNA family, is suggested to have an oncogenic role in cancers. For instance, MIR155HG inhibition suppressed proliferation and enhanced apoptosis of pancreatic cancer cells [21]. Moreover, MIR155HG promoted M1 macrophage polarization and therefore aggravated inflammatory response in chronic obstructive pulmonary disease [22]. However, the function of MIR155HG in CRC remains controversial since evidence for the exact role of MIR155HG and related mechanism in CRC is insufficient. In a study for evaluating the prognostic effects of lncRNAs in CRC, MIR155HG was found to be down-regulated in tumor tissues and lower MIR155HG expression was associated with poorer prognosis [23]. Meanwhile, Wu et al. found that MIR155HG-related single-nucleotide polymorphisms affected the susceptibility of Han Chinese population to CRC [24]. A conclusion drawn from Wu's study is that MIR155HG might likely increase the risk of CRC.

LncRNAs are frequently observed in competitive regulatory interactions where they act as microRNA (miRNA) decoys to modulate gene expression [25]. A previous study showed that MIR155HG competed with annexin A2 (ANXA2) for binding miR-185 and promoted glioblastoma growth by increasing the expression of ANXA2 [26]. ANXA2 is a well-characterized protein in cancer progression and is generally associated with adverse outcome and poor prognosis of cancer patients [27]. Moreover, ANXA2 was overexpressed in CRC tissues and promoted TGF-β-induced invasiveness of CRC cells [28]. In this study, we verified whether MIR155HG mediated the expression of ANXA2 by the competitive regulatory mechanism in CRC and whether this interaction was associated with CRC development.

Materials and methods

Tissue samples

CRC and adjacent noncancerous tissues were surgically removed from 45 patients with rectal cancer and 22 patients with colon cancer (35 males and 32 females; 42 ~ 76 years old with an average age of 66.73 ± 9.27 years) at Xiangya Hospital, Central South University from June 2018 to March 2019. Inclusion criteria: (1) diagnosed with CRC after preoperative colonoscopy and biopsy; (2) primary diagnosis; and (3) in the absence of preoperative radiotherapy, chemotherapy or any other anti-tumor treatment. Exclusion criteria: (1) complicated with other malignant tumors; (2) recurrent CRC; (3) family history of CRC, (4) suspected Lynch syndrome; and (5) breastfeeding or pregnant women. Among the selected patients, 24 had history of smoking and 29 had history of alcohol drinking. There were 36 cases with lymph node metastasis (LNM) and 31 cases without. All isolated samples were immediately placed into liquid nitrogen and preserved for later use. The sample acquisition obtained approval from the Ethics Committee of Xiangya Hospital, Central South University and informed consents from all patients or their families.

Cell cultivation

Human CRC cell lines (SW480, Caco2, HT29, HCT116 and LoVo), normal colorectal epithelial cells (HCoEpiC) and THP-1 cells were purchased from American Type Culture Collection (Manassas, Virginia, USA) and cultured in DMEM (Gibco, Grand Island, NY, USA) containing 10%

fetal calf serum (FBS) and 1% penicillin/streptomycin at 37 °C with 5% CO_2.

Cell transfection

Design and synthesis of shRNA against MIR155HG (sh-MIR155HG; forward sequence 5'-CCGGGGTGATGTGTCAACTTCAACCCTCGAGGGTTGAAGTTGACACATCACCTTTTTG-3'), shRNA against ANXA2 (sh-ANXA2; forward sequence 5'-CCGGCGGGATGCTTTGAACATTGAACTCGAGTTCAATGTTCAAAGCATCCCGTTTTTG-3'), negative control shRNA (sh-NC), pcDNA3.1-ANXA2 (ANXA2), pcDNA3.1 (vector), miR-650 mimic (mimic) and mimic-NC were all conducted by GenePharma (Shanghai, China). Cell transfection was performed using Lipofectamine 2000 reagent (Invitrogen, Carlsbad, CA, USA) following the instruction. The dosage of shRNA or pcDNA3.1 vectors was set at 2 μg, and the dosage of miR-650 mimic or mimic-NC was set at 50 nM. Cells with transfection efficiency over 70% were selected for following experiments which were performed within three days after transfection.

qRT-PCR

The total RNA was extracted from the tissues and cells using TRIzol-based method (Invitrogen, Carlsbad, CA, USA). Reverse transcription (RT) was conducted in RT reagent kit (TaKaRa, Tokyo, Japan) based on the instruction. Gene expressions were detected by LightCycler 480 (Roche, Indianapolis, IN, USA), and the reaction system was set according to the instruction of a fluorescence quantitative PCR kit (SYBR Green Mix, Roche Diagnostics, Indianapolis, IN). Below were parameters of thermal cycling: 95 °C, 10 s; 95 °C (5 s), 60 °C (10 s), 72 °C (10 s), 45 cycles in total; 72 °C, 5 min. Each RNA sample was tested in triplicate with GAPDH acting as the internal reference. The $2^{-\Delta\Delta Ct}$ method was used for data analysis. $\Delta\Delta Ct = (Ct_{\text{target gene}} - Ct_{\text{reference gene}})_{\text{experimental group}} - (Ct_{\text{target gene}} - Ct_{\text{reference gene}})_{\text{control group}}$. Primer sequences of genes used for PCR are shown in Table 1.

Western blotting

RIPA lysis buffer was used for protein extraction. Proteins were quantified by BCA kit (Beyotime). Proteins of required volume were mixed with loading buffer (Beyotime) and denatured in boiling water for 3 min. Electrophoresis was run at 80 V for 30 min until bromophenol blue entered the separation gel, and then the electrophoresis was continued at 120 V for 1 ~ 2 h. Proteins were transferred to a membrane at 300 mA, on ice for 60 min. The membrane was washed for 1 ~ 2 min and confined in blocking buffer at room temperature for 60 min or at 4 °C overnight. The proteins were incubated with primary antibodies of ANXA2 (8235S, 1:1000), IL-1β (12703S, 1:1000), iNOS (39898S, 1:1000), CD206 (91992S, 1:1000), Arginase-1 (93668S, 1:1000), IL-10 (12163S, 1:1000), MDR1 (13978S, 1:1000), MRP2 (4446S, 1:1000), GAPDH (5174S, 1:1000) (Cell Signaling, Boston, USA) on a shaking bed at room temperature for 1 h. After 3 × 10 min washing, the membrane was transferred to secondary antibody solution and shaken at room temperature for 1 h. The membrane was again washed for 3 × 10 min. The proteins were visualized using developing solution and detected by a chemiluminescence imaging system (Bio-Rad, Hercules, CA, USA).

Table 1 Primer sequences

Name of primer	Sequences
miR-650-F	AGGAGGCAGCGCTCT
miR-650-R	TGGTGTCGTGGAGTCG
U6-F	CTCGCTTCGGCAGCACA
U6-R	AACGCTTCACGAATTTGCGT
MIR155HG-F	CCACCCAATGGAGATGGCTC
MIR155HG-R	AGTTGGAGGCAAAAACCCCT
ANXA2-F	CACGGCCCAGGTTATCTTGT
ANXA2-R	TGCTGCGGTTGGTCAAAATG
IL-1β-F	CAGAAGTACCTGAGCTCGCC
IL-1β-R	AGATTCGTAGCTGGATGCCG
iNOS-F	CGCATGACCTTGGTGTTTGG
iNOS-R	CATAGACCTTGGGCTTGCCA
CD206-F	ACCTGCGACAGTAAACGAGG
CD206-R	TGTCTCCGCTTCATGCCATT
Arginase-1-F	ACTTAAAGAACAAGAGTGTGATGTG
Arginase-1-R	CATGGCCAGAGATGCTTCCA
IL-10-F	TGTTGCCTGGTCCTCCTGAC
IL-10-R	TGGGTCTTGGTTCTCAGCTTG
MDR1-F	ACTCACTTCAGGAAGCAACC
MDR1-R	CTTGGAAGAGCCGCTACTCG
MRP2-F	TGCATCTAGGCAAGGTTAACGA
MRP2-R	AGGAGCCATAGGTAGCCCAA
NEAT1-F	GGCAGGTCTAGTTTGGGCAT
NEAT1-R	CCTCATCCCTCCCAGTACCA
GAPDH-F	AATGGGCAGCCGTTAGGAAA
GAPDH-R	GCGCCCAATACGACCAAATC

F forward, *R* reverse

CCK-8 assay

Caco2 and HT29 cells of each group were seeded into 96-well plates with each well filled with 100 μl of diluted cell suspension (1×10^5 cells/ml). Each group had three duplicates. After 0, 24, 48, 72 and 96-h incubation, each well

was added with 10 µl of CCK-8 reagent (Tokyo, Dojindo, Japan). OD450 (optical density at 450 nm) was measured after 2-h incubation with CCK-8 reagent.

Colony formation assay

Caco2 and HT29 cells of each group were digested by pancreatin and centrifuged at 1500 rpm, 25 °C for 5 min. Cells were resuspended in complete medium and seeded in 6-well plates filled with 2 ml of 37 °C complete medium with each well containing 500 cells. Cells were cultured for 2 ~ 3 weeks (37 °C, 5% CO_2) until there were visible cell colonies in the plate. After that, medium in the plate was cleared and the plate was washed with PBS. Each well was added with 1.5 ml methanol for 15 min of cell fixation. The methanol was then cleared and 1 ml of Giemsa staining solution was added along the well wall. After 20-min staining in the dark, the staining solution was washed off by running water. The plate was put upside down and dried on clean absorbent paper.

Scratch assay

Caco2 and HT29 cells of each group were seeded in 6-well plates with each well containing 2×10^6 cells. Each group had three duplicates. Cells were cultured at 37 °C with 5% CO_2 for 24 h until the well was fully covered by a single layer of cells. These cells were scratched by a 200 µ1 sterile pipette tip. After PBS wash, the cells were cultured in at 37 °C with 5% CO_2 for another 24 h. The position of scratches after 0 and 24 h was photographed under a microscope. Migration rate = (scratch position at 0 h-scratch position at 24 h)/scratch position at 0 h.

Transwell invasion assay

Caco2 and HT29 cells of each group were resuspended in serum-free medium. The Matrigel-coated apical chamber of Transwell plate (354,480, Corning, NY, USA) was seeded with 100 µ1 of cells (3×10^5) and the basolateral chamber was added with 600 µ1 of 10% FBS. After 24-h incubation at 37 °C, medium in the apical chamber was removed and the remaining cells were cleared using a wet swab. Cells in the basolateral chamber were fixed in 4% paraformaldehyde for 30 min and then stained with Giemsa staining solution for 20 min. The number of cells that had invaded into the basolateral chamber was counted under a microscope.

Macrophage polarization

THP-1 cells were induced by PMA (100 ng/ml, 24 h; Sigma-Aldrich, Merck KGaA, Darmstadt, Germany) to differentiate into macrophages. THP-1-derived macrophages were placed in the conditioned medium of transfected Caco2 and HT29 cells before polarization. M1 or M2 macrophages were induced by LPS (1 µg/ml, Sigma-Aldrich, Merck KGaA, Darmstadt, Germany) + IFN-γ (50 ng/ml, R&D Systems, Minneapolis, MN, USA) or IL-4 + IL-13 (20 ng/ml, R&D Systems, Minneapolis, MN, USA) for 24 h.

Flow cytometry

The expressions of non-specific macrophage marker (CD68), M1 macrophage marker (CD11c) and M2 macrophage marker (CD206) were measured by a flow cytometer (EXL™, Beckman Coulter) to determine the percentages of total macrophages ($CD68^+$), M1 macrophages ($CD68^+CD11c^+$) or M2 macrophages ($CD68^+CD206^+$) in each group. PMA-induced macrophages (1×10^6) were incubated with FITC-marked CD68 antibody (ab134351, 10 µl, Abcam, Cambridge, MA, USA). Macrophages induced by LPS + IFN-γ were incubated with FITC-marked CD68 antibody and PerCP/Cy5.5®-marked CD11c antibody (ab233643, 4 µl, Abcam, Cambridge, MA, USA). Macrophages induced by IL-4 + IL-13 were incubated with FITC-marked CD68 antibody and APC-marked CD206 antibody (ab223961, 20 µl, Abcam, Cambridge, MA, USA).

Oxaliplatin treatment

Caco2 and HT29 cells were incubated in the conditioned medium of M2 macrophages or PBS for 8 h and then treated with oxaliplatin (Sanofi-Synthelabo, NY, USA) for 24 h. CCK-8 and colony formation assays were applied to assess the oxaliplatin sensitivity of these cells. CCK-8 assay measured OD450 in Caco2 and HT29 cells after oxaliplatin treatment at different concentrations (0, 1, 5, 10, 20 and 100 µM). Colony formation assay detected the colonies of Caco2 and HT29 cells after 20 µM oxaliplatin treatment for 24 h.

Location of MIR155HG

Cytoplasmic & Nuclear RNA Purification kits (Norgen Biotek, Thorold, ON, Canada) were used to extract RNA from the cytoplasm and nucleus of Caco2 and HT29 cells. qRT-PCR detected the expression of MIR155HG to determine the subcellular localization of MIR155HG in Caco2 and HT29 cells. GAPDH served as the internal reference of cytoplasmic MIR155HG and nuclear enriched abundant transcript 1 (NEAT1) acted as the internal reference of nuclear MIR155HG.

RNA immunoprecipitation (RIP)

Cells were washed with pre-cooled PBS for twice before being centrifuged at 1,500 rpm for 5 min. Cells were then

mixed with equal amount of RIP Lysis Buffer in the centrifugation tube. Magnetic beads were resuspended in 100 µl of RIP Wash Buffer and incubated with 5 µg of Ago2 antibody (ab32381, 1:100, Abcam, Cambridge, MA, USA) at room temperature for 30 min; the negative control group was incubated with IgG antibody. The centrifugation tube was placed on a magnetic grate with supernatant discarded. The tube was added with 500 µl of RIP Wash Buffer and supernatant was discarded after vortex oscillation. This step was repeated. The tube was added with 500 µl of RIP Wash Buffer and placed on ice after vortex oscillation. The magnetic bead tube was placed on the magnetic grate with supernatant discarded and then added with 900 µl of RIP Immunoprecipitation Buffer. The cell lysate was rapidly thawed and centrifuged at 14,000 rpm, 4 °C for 10 min. The bead-antibody complexes were incubated with 100 µl of supernatant at 4 °C overnight. After a short centrifugation, the centrifugation tube was placed on a magnetic grate with supernatant discarded. The tube was added with 500 µl of RIP Wash Buffer and placed on the magnetic grate after vortex oscillation. The supernatant was discarded and the remaining complexes were washed for six times. The bead-antibody complexes were resuspended in 150 µl of Proteinase K Buffer and incubated at 55 °C for 30 min. After that, the bead tube was placed on the magnetic grate. qRT-PCR detected the expression of RNAs which were extracted from the supernatant.

Dual-luciferase reporter assay

The binding sites of MIR155HG/miR-650, miR-650/ANXA2 and MIR155HG/ANXA2 were predicted by starBase (http://starbase.sysu.edu.cn/). Wild and mutated sequences of the binding sites were designed and synthesized according to the prediction. Sequence names were as follows: wt-MIR155HG & mut-MIR155HG (wild and mutated sequences of the binding site between MIR155HG and miR-650), wt-ANXA2 & mut-ANXA2 (wild and mutated sequences of the binding site between miR-650 and ANXA2) and WT-MIR155HG & MUT-MIR155HG (wild and mutated sequences of the binding site between MIR155HG and ANXA2). The sequences were inserted into pGL3-Promoter vectors and then co-transfected with miR-650 mimic, the 3'UTR sequence of ANXA2 mRNA or negative control into HEK293T cells or pRL-TK vector (internal reference). After transfection, the activities of Firefly luciferase and Renilla luciferase (internal reference) were detected. Relative luciferase activity = Firefly luciferase activity/Renilla luciferase activity.

RNA pull-down

RNA pull-down assay was applied to verify the binding between MIR155HG and ANXA2. Biotin-labeled MIR155HG probe or scramble probe (Takara, Tokyo, Japan) was incubated with cell lysate and then incubated with streptavidin-coated magnetic beads (Invitrogen, Carlsbad, CA, USA). RNAs were isolated from the complexes captured by magnetic beads. qRT-PCR detected the mRNA level of ANXA2.

Stability test of mRNA

Actinomycin D (1 µg/ml, Sigma-Aldrich, St. Louis, USA) was used to inhibit gene transcription in Caco2 and HT29 cells. qRT-PCR detected mRNA level of the remaining ANXA2 in cells collected after 0, 1, 3, 5, 7 and 9 h of actinomycin D treatment.

Fluorescence in situ hybridization (FISH)

Fluorescence-labeled probes were placed in a 75 °C water bath for 5 min and then immediately placed at 0 °C for 5 ~ 10 min to denature double-stranded DNA. Prepared cell slides were baked at 50 °C for 2 ~ 3 h and then immersed in 70% formamide/2 × SSC denaturation solution (70 ~ 75 °C) for 2 ~ 3 min. The slides were sequentially soaked in 70%, 90%, and 100% ice ethanol for 5 min each time and then air-dried. The slides were added with 10 µl of the denatured DNA probes, covered with cover glass, and placed in a humidified dark box at 37 °C overnight. After that, the slides were washed 3 times with 50% formamide/2 × SSC (42 ~ 50 °C, 5 min each time), 3 times with 1 × SSC (42 ~ 50 °C, 5 min each time), and once with 2 × SSC at room temperature. Air-dried slides were added with 200 µl of counterstain (DAPI/antifade solution), covered with cover glass, and observed under a fluorescence microscope.

Animal experiment

Specific pathogen free (SPF) BALB/c nude mice ($n = 36$, 4 ~ 6 weeks, 16 ± 2 g) were obtained from Shanghai Experimental Animal Center, Chinese Academy of Sciences. All mice were raised in SPF laminar airflow bioclean room at 22 ~ 26 °C with 55 ± 5% humidity. All animal experiments abided by the rules and operation norms of laboratory animal management and relevant ethical requirements of laboratory animals. Mice were randomized into six groups and anesthetized by pentobarbital sodium (60 mg/kg) and ketamine (50 mg/kg). After anesthetization, mice in the sh-NC group, sh-MIR155HG group and sh-ANXA2 group were subcutaneously injected at the right back with 1×10^6 Caco2 or HT29 cells, puromycin-selected Caco2 or HT29

cells in which MIR155HG was stably underexpressed, and puromycin-selected Caco2 or HT29 cells in which ANXA2 was stably underexpressed, respectively. The tumor size was measured at regular intervals. Mice were killed four weeks later and tumors were isolated. Tumor size = 1/2 × long diameter × short diameter ^{2}. After the measurement of tumor size, the tumors were paraffin-embedded and sliced.

Immunohistochemistry

Isolated tumors were fixed in 4% paraformaldehyde for 48 h and then made into paraffin sections. (4 μm). The tumor sections were roasted for 20 min, dewaxed in routine xylene and washed with distilled water. After three PBS washes, the tumor tissues were treated with 3% H_2O_2 at room temperature for 10 min. The tissues were washed with PBS for three times and then subjected to thermal antigen retrieval. After another round of PBS washes, the tissues were blocked in normal goat serum blocking buffer at room temperature for 20 min. Access blocking buffer was removed and the tissues were incubated with primary antibodies of Ki-67 (12202S, 1:400) and CD206 (91992S, 1:400) (Cell Signaling, Boston, USA) at 4 °C overnight. The tissues were washed with PBS for three times and then incubated with secondary antibody at room temperature for 1 h. After three PBS washes, the tissues were treated with DAB for 1 ~ 3 min and hematoxylin for 3 min. After tissue dehydration and transparentization, the slides were mounted.

Statistical analysis

Data were analyzed in GraphPad prism7 and finally presented as mean ± standard deviation (SD). Two-group comparison, multi-group comparison and multiple comparisons post hoc were conducted using *T* test, One-way analysis of variance and Tukey's multiple comparisons test, respectively. Kaplan–Meier and Chi-squared tests were used to analyze the relation between the expressions of MIR155HG/ANXA2 and the prognosis and pathological characteristics of CRC patients. Pearson correlation analysis was applied for the expressions of MIR155HG and ANXA2 in CRC tissues. $P < 0.05$ was deemed statistically significant.

Results

LncRNA MIR155HG and ANXA2 are overexpressed in human CRC tissues

The Cancer Genome Atlas (TCGA) database showed that ANXA2 had higher expressions in colon adenocarcinoma (COAD) and rectum adenocarcinoma (READ) than in noncancerous tissues (Fig. 1a, $P < 0.05$). Meanwhile, the expressions of MIR155HG and ANXA2 were positively correlated in COAD and READ (Fig. 1b, $P < 0.05$). We detected the expressions of MIR155HG and ANXA2 in collected CRC and para-carcinoma tissues ($n = 67$) using qRT-PCR. The results showed increases in the expressions of MIR155HG and ANXA2 in CRC tissues (Fig. 1c, d, $P < 0.01$). Also, the expressions of MIR155HG and ANXA2 were positively correlated in CRC tissues (Fig. 1e, $P < 0.05$).

The CRC patients were divided into low expression group ($n = 33$) and high expression group ($n = 34$) by the median value of the expression of MIR155HG or ANXA2. The association between the expressions of MIR155HG/ANXA2 and pathological characteristics of CRC patients are shown in Tables 2 and 3. The expression of MIR155HG or ANXA2 was not related to the sex or age of CRC patients. MIR155HG expression was significantly associated with the tumor size and LNM of CRC patients (Table 2) and ANXA2 expression was linked to the tumor size and tumor differentiated degree (Table 3). Kaplan–Meier survival analysis showed that the overall 5-year survival of patients with high expression of MIR155HG (Fig. 1f, $P < 0.05$) or ANXA2 (Fig. 1g, $P < 0.01$) was significantly lower than that of the patients in low expression group. The above analysis indicated that MIR155HG and ANXA2 exerted oncogenic effect in CRC.

Knockdown of lncRNA MIR155HG or ANXA2 suppresses cellular activities of CRC cells

The expressions of MIR155HG and ANXA2 in CRC cell lines (SW480, Caco2, HT29, HCT116 and LoVo) and normal colorectal epithelial cells (HCoEpiC) were measured by qRT-PCR and Western blotting. MIR155HG and ANXA2 were highly expressed in CRC cell lines compared with HCoEpiC cells (Fig. 2a–c, $P < 0.05$). To investigate the effects of MIR155HG and ANXA2 on CRC cells, Caco2 and HT29 cells were transfected with sh-MIR155HG (sh-MIR155HG group), sh-ANXA2 (sh-ANXA2 group) or sh-MIR155HG + pcDNA3.1-ANXA2 (sh-MIR155HG + ANXA2 group). The transfection efficiency of each group was above 70% (Fig. S1). MIR155HG and ANXA2 were down-regulated in the sh-MIR155HG group; ANXA2 was down-regulated while MIR155HG expression had no significant differences in the sh-ANXA2 group (Fig. 2d–f, $P < 0.05$, vs. the sh-NC group). This suggested that MIR155HG positively regulated the expression of ANXA2.

CCK-8 assay showed that the viability of Caco2 and HT29 cells with down-regulated MIR155HG or ANXA2 was impaired while overexpressing ANXA2 reversed the suppression of MIR155HG knockdown on cell viability (Fig. 2g, $P < 0.05$). Clones formed by Caco2 and HT29 cells with down-regulated MIR155HG or ANXA2 were

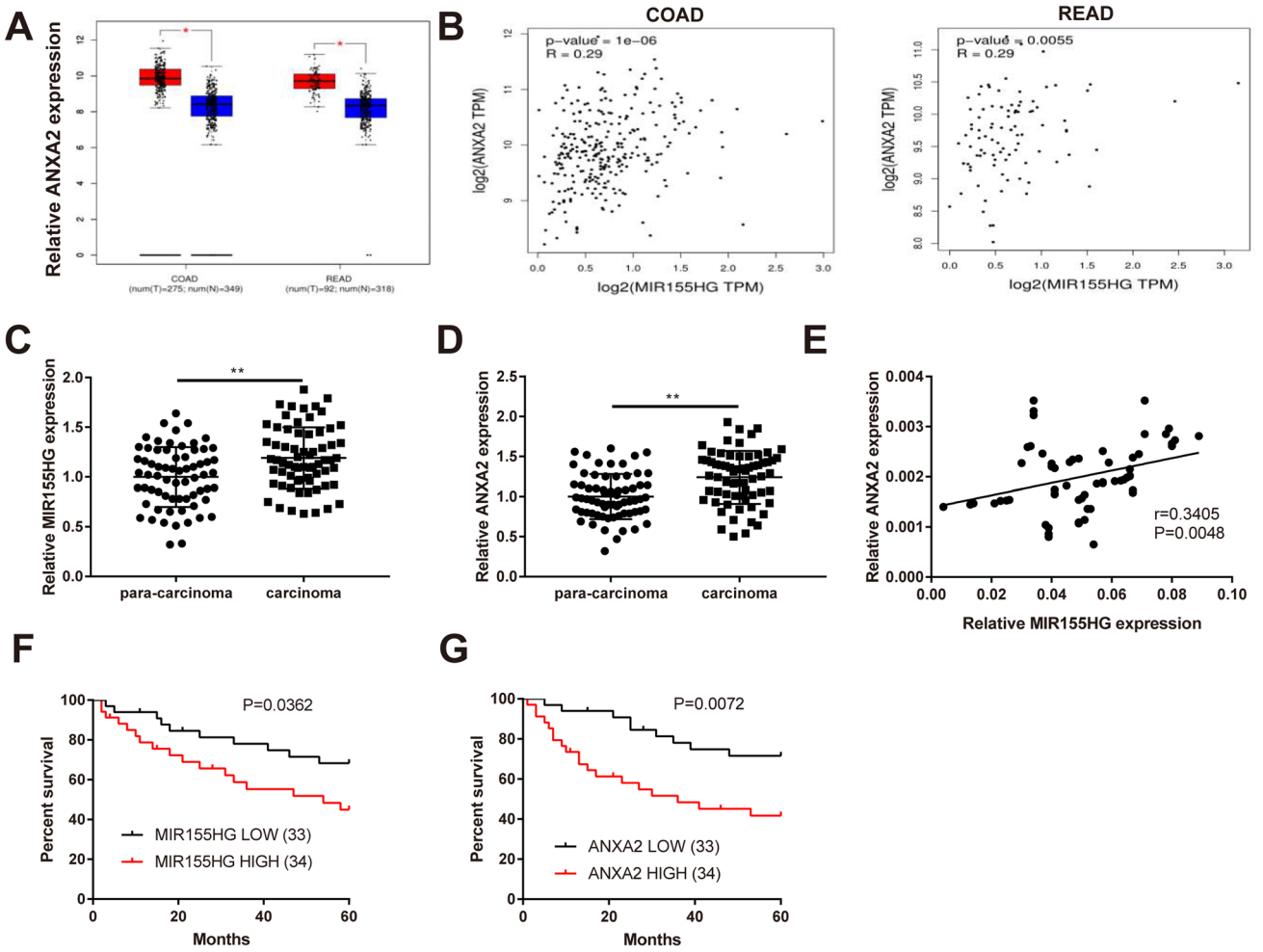

Fig. 1 LncRNA MIR155HG and ANXA2 are highly expressed in CRC tissues. Notes: **a** ANXA2 was highly expressed in COAD and READ in TCGA database; **b** the expressions of MIR155HG and ANXA2 were positively related in COAD and READ in TCGA database; **c**–**d** the mRNA levels of MIR155HG and ANXA2 in 67 CRC tissue samples; **e** correlation analysis of the expressions of MIR155HG and ANXA2 in collected CRC tissue samples; **f**–**g** survival analysis of patients with low or high expressions of MIR155HG and ANXA2. $^{**}P < 0.01$; CRC, colorectal cancer

Table 2 Association between MIR155HG expression and pathological characteristics of CRC patients

Pathological characteristics	MIR155HG LOW (33)	MIR155HG HIGH (34)	*P*
Gender (F/M)	15/18	17/17	0.8083
Age (< 60/≥ 60)	10/23	12/22	0.7959
Tumor size (< 3/≥ 3 cm)	21/12	12/22	0.0283*
TNM (I/II/III/IV)	3/13/12/5	4/14/12/4	0.9645
Differentiated degree (poor/moderate/well)	9/16/8	13/15/6	0.5973
Lymph node metastasis (no/yes)	20/13	11/23	0.0280*

CRC colorectal cancer, *F* female, *M* male. $^{*}P < 0.05$

significantly reduced while overexpressing ANXA2 abolished the suppressive effect of MIR155HG knockdown on cell clonality of Caco2 and HT29 cells (Fig. 2h, $P < 0.05$). Scratch assay showed that the migration rates of Caco2 and HT29 cells were decreased in the sh-MIR155HG group and sh-ANXA2 group (vs. the sh-NC group) while increased in the sh-MIR155HG + ANXA2 group (vs. the sh-MIR155HG group) (Fig. 2i, $P < 0.05$).

Table 3 Association between ANXA2 expression and pathological characteristics of CRC patients

Pathological characteristics	ANXA2 LOW (33)	ANXA2 HIGH (34)	*P*
Gender (F/M)	14/19	18/16	0.4664
Age (< 60/≥ 60)	8/25	14/20	0.1944
Tumor size (< 3/≥ 3 cm)	22/11	11/23	0.0072**
TNM (I/II/III/IV)	3/12/14/4	4/15/10/5	0.7436
Differentiated degree (poor/moderate/well)	6/20/7	16/11/7	0.0281*
Lymph node metastasis (no/yes)	18/15	13/21	0.2242

CRC colorectal cancer, *F* female, *M* male. *$P < 0.05$, **$P < 0.01$

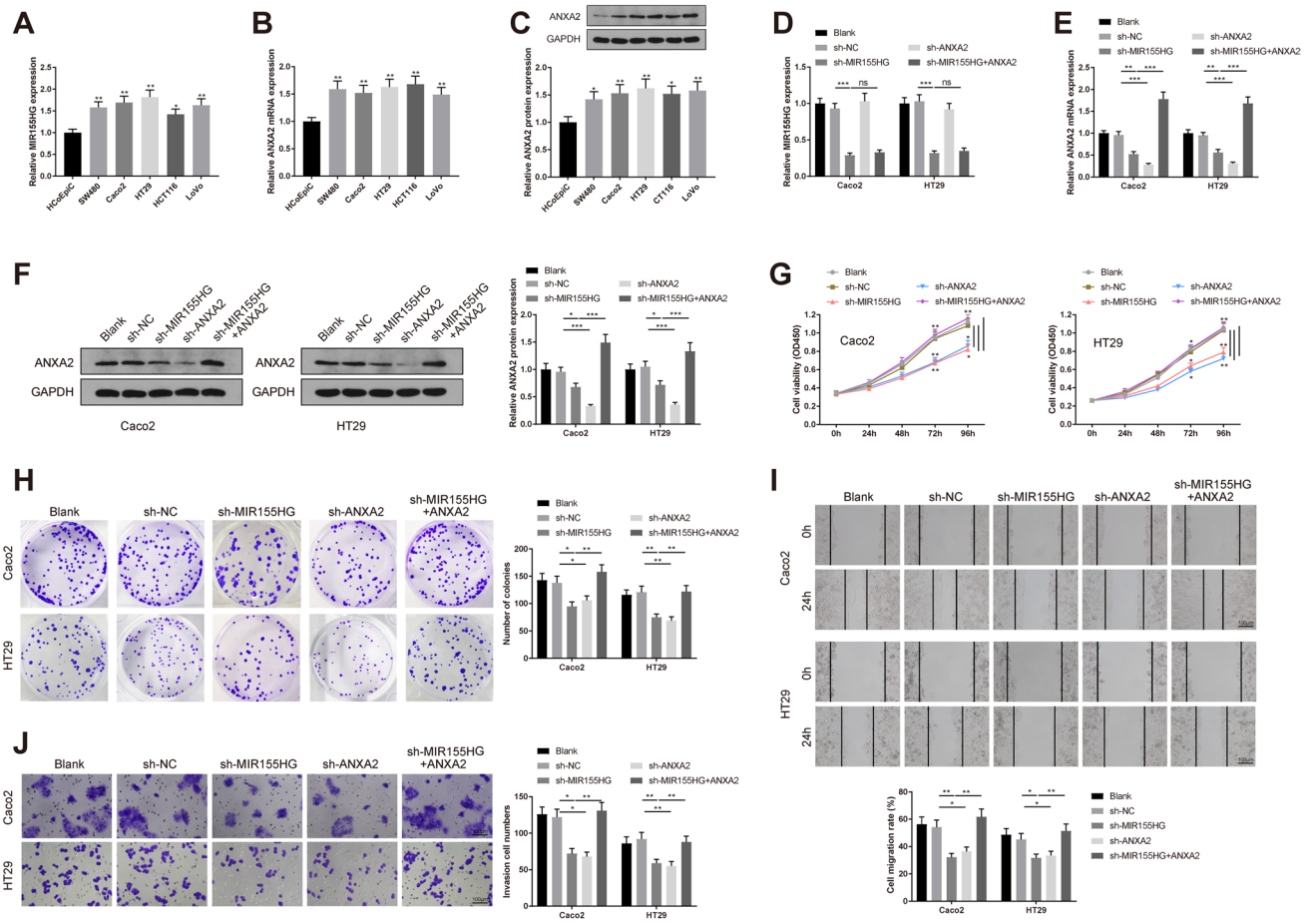

Fig. 2 Knockdown of lncRNA MIR155HG or ANXA2 suppresses proliferation, migration and invasion of CRC cells. Notes: The expressions of MIR155HG (**a**) and ANXA2 (**b–c**) in CRC cells. After cell transfection, the expressions of MIR155HG (**d**) and ANXA2 (**e–f**) in Caco2 and HT29 cells were detected; **g** CCK-8 tested the viability of Caco2 and HT29 cells; **h** colony formation assay measured the number of cell clones; **i** scratch assay assessed the migration rate of Caco2 and HT29 cells; **j** Transwell assay assessed the invasive ability of Caco2 and HT29 cells. *$P < 0.05$, **$P < 0.01$, ***$P < 0.001$; CRC, colorectal cancer

The invasive ability of Caco2 and HT29 cells incubated in Transwell plates was hampered in the sh-MIR155HG group and sh-ANXA2 group (vs. the sh-NC group) while improved in the sh-MIR155HG + ANXA2 group (vs. the sh-MIR155HG group) (Fig. 2j, $P < 0.05$). The above experiment data suggested that MIR155HG and ANXA2 could promote the proliferation, migration and invasion of CRC cells.

Knockdown of lncRNA MIR155HG or ANXA2 in CRC cells inhibits M2 macrophage polarization

PMA-induced macrophages were incubated with the conditioned medium of CRC cells from the sh-NC group, sh-MIR155HG group, sh-ANXA2 group or sh-MIR155HG + ANXA2 group and accordingly divided into sh-NC-CM group, sh-MIR155HG-CM group, sh-ANXA2-CM group or sh-MIR155HG + ANXA2-CM group. Then these macrophages were treated with LPS + IFN-γ or IL-4 + IL-13 to activate M1 or M2 phenotype. The following experiments were performed to evaluate the effect of MIR155HG or ANXA2 knockdown on macrophage polarization. qRT-PCR and Western blotting were applied to measure the expressions of M1 macrophage markers (IL-1β and iNOS) and M2 macrophage markers (CD206, Arginase-1 and IL-10). The expressions of IL-1β and iNOS experienced no significant changes in LPS + IFN-γ-induced M1 macrophages (Fig. 3a, b, $P > 0.05$).

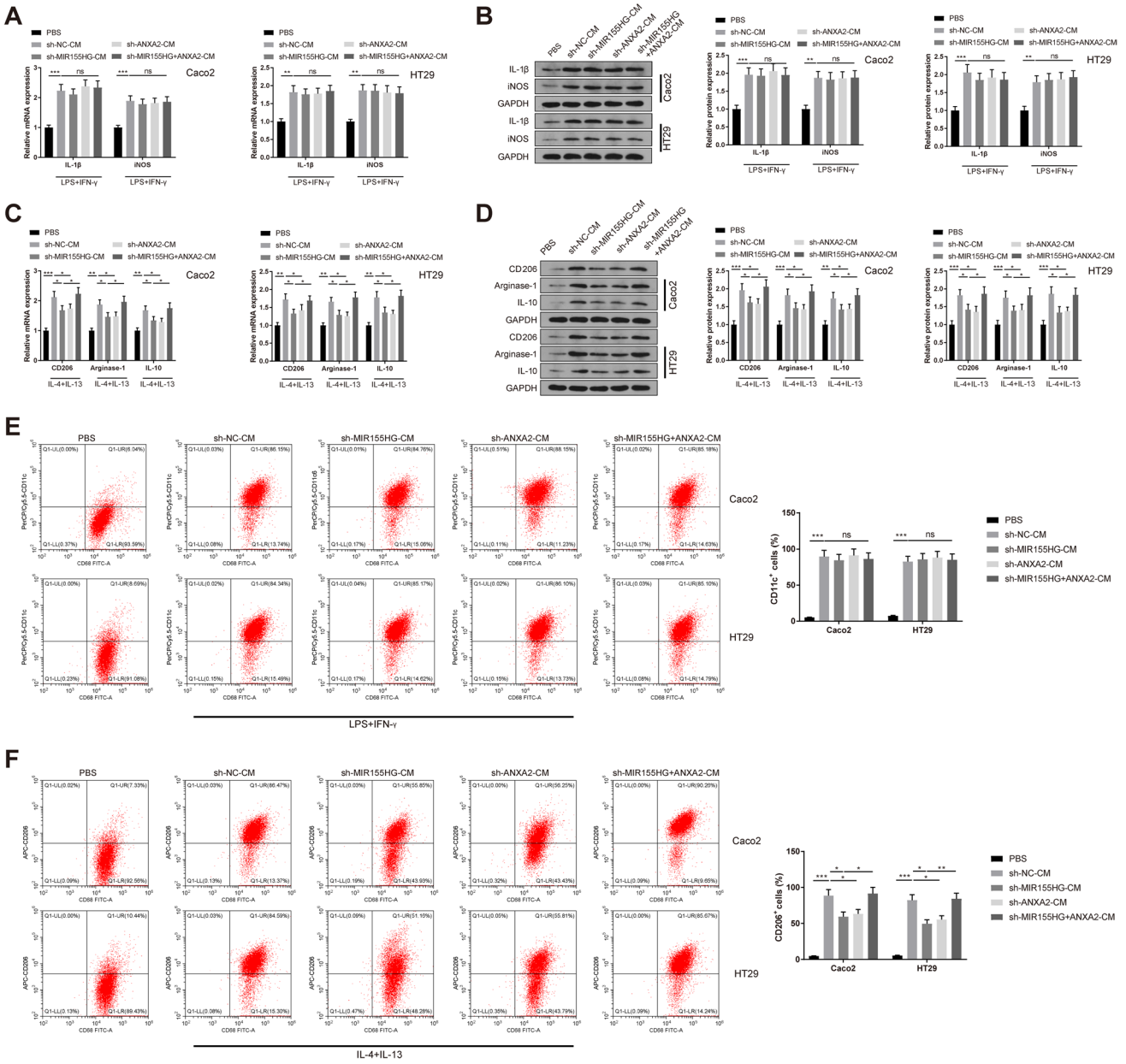

Fig. 3 Knockdown of lncRNA MIR155HG or ANXA2 inhibits M2 polarization of macrophages. Notes: PMA-induced THP-1 macrophages were incubated with CM of the sh-MIR155HG group, sh-ANXA2 group or sh-MIR155HG + ANXA2 group and then treated with LPS + IFN-γ or IL-4 + IL-13. **a**–**b** The expressions of IL-1β and iNOS in macrophages after M1 induction; **c**–**d** the expressions of CD206, Arginase-1 and IL-10 in macrophages after M2 induction; **e** the portion of M1 macrophages; **f** the portion of M2 macrophages. $^{*}P < 0.05$, $^{**}P < 0.01$, $^{***}P < 0.001$

CD206, Arginase-1 and IL-10 were significantly reduced in IL-4 + IL-13-induced M2 macrophages of the sh-MIR155HG-CM group and sh-ANXA2-CM group (vs. the sh-NC-CM group) while increased in the sh-MIR155HG + ANXA2-CM group (vs. the sh-MIR155HG-CM group) (Fig. 3c, d, $P < 0.05$). According to the measurement of the expressions of surface markers CD68 (all macrophages), CD206 (M2 macrophages) and CD11c (M1 macrophages) by flow cytometry, the portion of $CD68^+CD11c^+$ macrophages in each group had no significant changes after LPS + IFN-γ treatment (Fig. 3e, $P > 0.05$). $CD68^+CD206^+$ macrophages were reduced in the sh-MIR155HG-CM group and sh-ANXA2-CM group while increased in the sh-MIR155HG + ANXA2-CM group (Fig. 3f, $P < 0.05$). Taken together, MIR155HG or ANXA2 inhibition could suppress the M2 polarization of macrophages but not affect M1 phenotype transformation.

Knockdown of lncRNA MIR155HG or ANXA2 attenuates oxaliplatin resistance of CRC cells by inhibiting M2 macrophage polarization

To determine the relation between M2 macrophage polarization and oxaliplatin resistance of CRC cells, Caco2 and HT29 cells were incubated with PBS or the conditioned medium of IL-4 + IL-13-induced M2 macrophages (M2-CM) of the above-mentioned groups and then treated with oxaliplatin. These cells were accordingly divided into PBS, sh-NC-M2-CM, sh-MIR155HG-M2-CM, sh-ANXA2-M2-CM, and sh-MIR155HG + ANXA2-M2-CM groups. CCK-8 assay showed that oxaliplatin-induced damage to the viability of Caco2 and HT29 cells was weakened in the sh-NC-M2-CM group in comparison with the PBS group (Fig. 4a, $P < 0.05$), which suggested that M2 macrophages enhanced the tolerance of Caco2 and HT29 cells to oxaliplatin. The viability of CRC cells was reduced in the sh-MIR155HG-M2-CM and sh-ANXA2-M2-CM groups when compared with the sh-NC-M2-CM group (Fig. 4a, $P < 0.05$). The colonies of the sh-NC-M2-CM group were increased compared with those of the PBS group, while the proliferation of CRC cells was suppressed in the sh-MIR155HG-M2-CM group and sh-ANXA2-M2-CM group compared with the sh-NC-M2-CM group (Fig. 4b, $P < 0.05$). Drug resistance-related genes MDR1 and MRP2 were increased in Caco2 and HT29 cells in the sh-NC-M2-CM group (vs the PBS group); the expressions of MDR1 and MRP2 were inhibited in the sh-MIR155HG-M2-CM group and sh-ANXA2-M2-CM group (vs. the sh-NC-M2-CM group) (Fig. 4c, d, $P < 0.05$). Collectively, M2 macrophage polarization mediates the susceptibility of CRC cells to oxaliplatin. Higher M2 polarization is of predictive value for stronger oxaliplatin resistance in CRC cells.

LncRNA MIR155HG competes with ANXA2 for miR-650

According to the sub-cellular localization of MIR155HG, MIR155HG was expressed in both the cytoplasm and nucleus of Caco2 and HT29 cells (Fig. 5a, $P < 0.05$). The results of FISH showed that MIR155HG and miR-650 were co-expressed in Caco2 and HT29 cells (Fig. 5b). miR-650 was found to be up-regulated in Caco2 and HT29 cells transfected with sh-MIR155HG (Fig. 5c, $P < 0.05$), suggesting that miR-650 can be negatively regulated by MIR155HG. Furthermore, ANXA2 was down-regulated in Caco2 and HT29 cells transfected with miR-650 mimic (Fig. 5d, e, $P < 0.05$), indicating that miR-650 can negatively regulate the expression of ANXA2.

RIP assay was applied to verify the binding between MIR155HG and miR-650 or ANXA2 and miR-650. MIR155HG and ANXA2 mRNAs were enriched in Ago2 antibody, instead of IgG antibody (Fig. 5f, $P < 0.05$), which indicated the direct binding between miR-650 and MIR155HG as well as direct interaction between ANXA2 and miR-650. To further determine the binding site between MIR155HG and miR-650 or ANXA2 and miR-650 with the application of dual-luciferase reporter assay, wild and mutated sequences of the binding sites were designed and synthesized (Fig. 5g). Cells inserted with wt-MIR155HG or wt-ANXA2 had significantly reduced luciferase activity (Fig. 5h, $P < 0.05$) while mut-MIR155HG or mut-ANXA2 did not impact on the luciferase activity (Fig. 5h). The above evidence demonstrated that MIR155HG up-regulated the expression of ANXA2 by competitively binding to miR-650.

LncRNA MIR155HG binds and stabilizes ANXA2 mRNA

Further, MIR155HG was demonstrated to be a direct sponge of ANXA2 mRNA. RNA pull-down assay showed that MIR155HG probes captured considerable ANXA2 mRNA while scrambled probes did not (Fig. 6a, $P < 0.05$). Binding sites between MIR155HG and ANXA2 mRNA predicted by starBase are shown in Fig. 6b. Cells inserted with WT-MIR155HG had increased luciferase activity (Fig. 6c, $P < 0.05$). The relative luciferase activity in cells inserted with MUT-MIR155HG experienced no significant changes. The results of dual-luciferase reporter assay indicated that MIR155HG could directly target ANXA2 mRNA. Actinomycin D was used to treat Caco2 and HT29 cells to investigate the influence of MIR155HG on stability of ANXA2 mRNA. The level of ANXA2 mRNA was detected at regular intervals. The degradation of ANXA2 mRNA was accelerated in Caco2 and HT29 cells with underexpressed MIR155HG (Fig. 6d, $P < 0.05$). Therefore, MIR155HG not only sponged ANXA2 mRNA but also stabilized it.

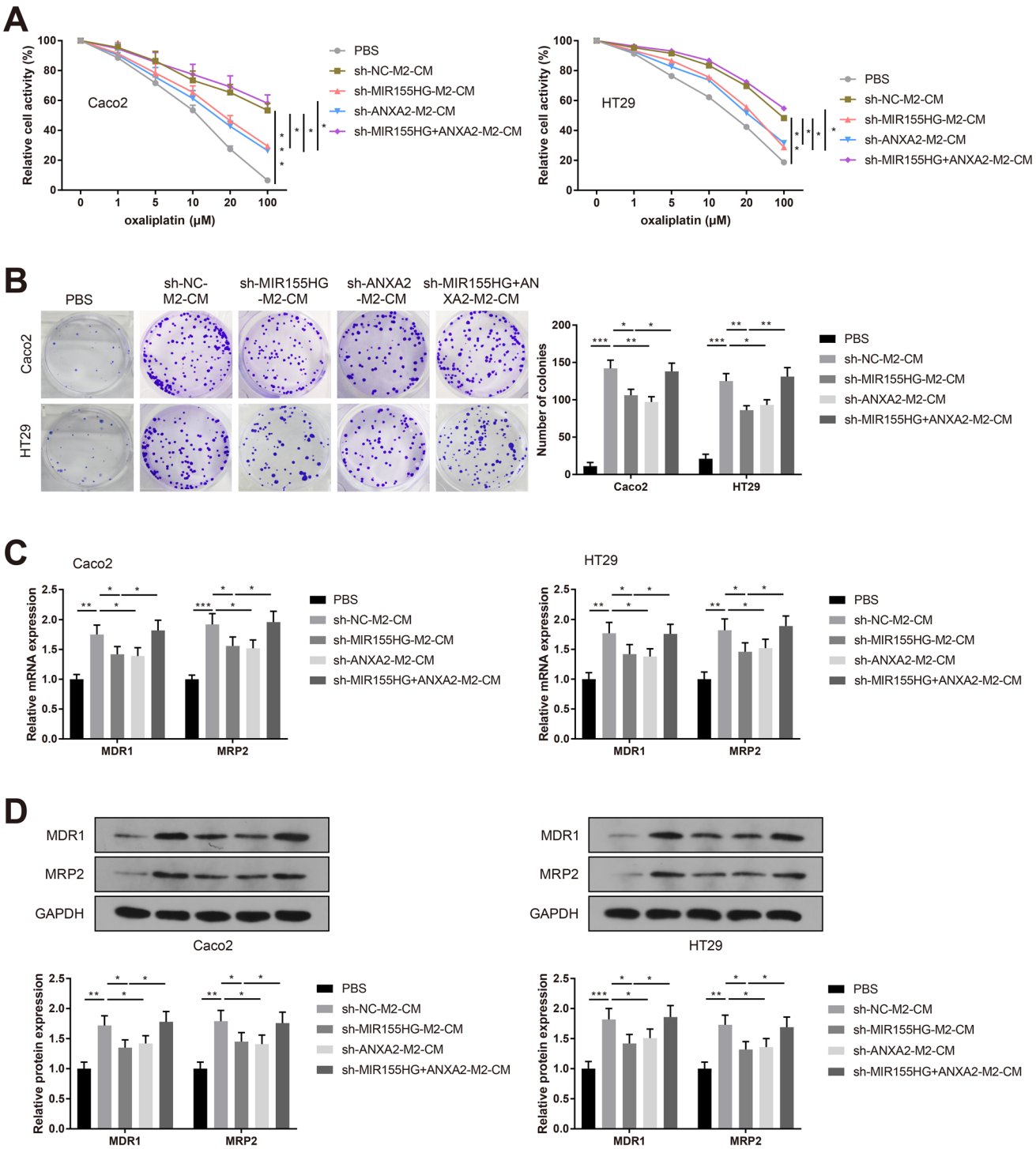

Fig. 4 Knockdown of lncRNA MIR155HG or ANXA2 attenuates oxaliplatin resistance of CRC cells. Notes: Caco2 and HT29 cells were incubated with PBS or M2 macrophage-CM of each group. **a** CCK-8 assay tested the toxicity of oxaliplatin to Caco2 and HT29 cells; **b** colony formation assay assessed the effect of oxaliplatin on clonality of Caco2 and HT29 cells; **c**–**d** the levels of drug resistance related genes MDR1 and MRP2. $^{*}P<0.05$, $^{**}P<0.01$, $^{***}P<0.001$; CRC, colorectal cancer

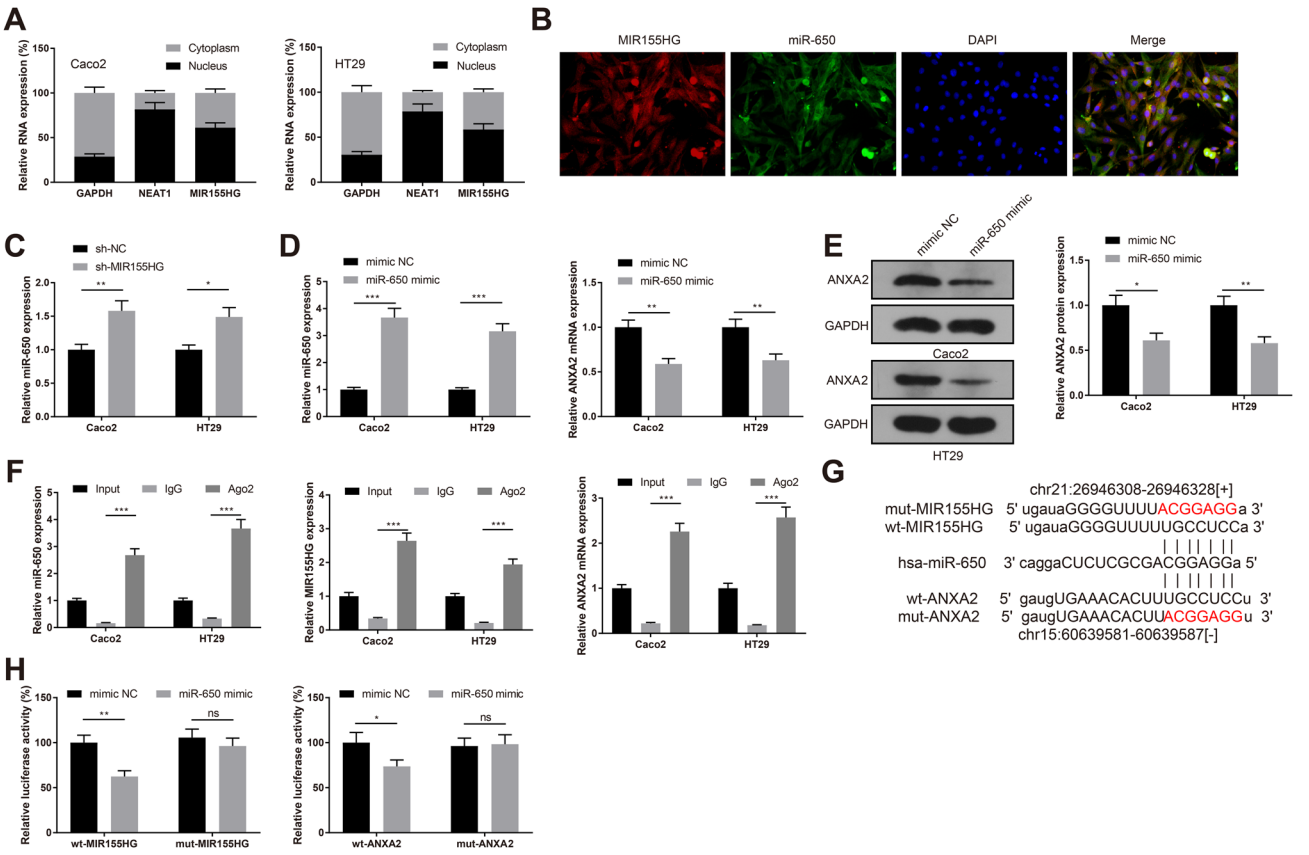

Fig. 5 LncRNA MIR155HG competes with ANXA2 for miR-650. Notes: **a** Sub-cellular localization of MIR155HG in Caco2 and HT29 cells; **b** co-localization of MIR155HG and miR-650; **c** the expression of miR-650 in Caco2 and HT29 cells transfected with sh-MIR155HG; **d–e** the expressions of miR-650 (**d**) and ANXA2 (**d–e**) in Caco2 and HT29 cells transfected with miR-65 mimic; **f** RIP assay verified the binding between MIR155HG and miR-650 or ANXA2 and miR-650; **g** binding site between MIR155HG and miR-650 or ANXA2 and miR-650 in starBase database; **h** dual-luciferase reporter assay verified the binding site between MIR155HG and miR-650 or ANXA2 and miR-650. $^{*}P<0.05$, $^{**}P<0.01$, $^{***}P<0.001$

Knockdown of lncRNA MIR155HG or ANXA2 inhibits CRC progression in nude mice

Nude mice were subcutaneously injected with Caco2 or HT29 cells with inhibited MIR155HG or ANXA2, or negative control Caco2 or HT29 cells to establish heterotopic xenograft models of human CRC. There were no significant differences in the general health and body weight of the mice from all these experimental groups. MIR155HG and ANXA2 were down-regulated in tumors of the sh-MIR155HG group; ANXA2 was down-regulated in tumors of the sh-ANXA2 group (Fig. 7a–c, $P<0.05$, vs. the sh-NC group). The volume of tumors was reduced in both the sh-MIR155HG group and sh-ANXA2 group (Fig. 7d, e, $P<0.05$, vs. the sh-NC group). Immunohistochemistry measured the numbers of Ki-67 and CD206-positive cells. Ki-67 and CD206-positive cells were decreased in the sh-MIR155HG group and sh-ANXA2 group (Fig. 7f, g, $P<0.05$, vs. the sh-NC group). In accordance with the cell experiments, the regulation of MIR155HG/ANXA2 in CRC was proved in vivo.

Discussion

CRC makes up a significant portion of all annually diagnosed cancers worldwide and the incidence and mortality vary geographically with the highest rates in developed countries. The incidence of CRC will increase as socioeconomic progress is continuing in developing countries [29]. Therefore, efforts are still needed to relieve the world burden and improve clinical outcomes of CRC. A novel axis, MIR155HG/ANXA2, in the progression of CRC was elucidated in the present study.

Firstly, we measured the expressions of MIR155HG and ANXA2 in collected CRC tissues. MIR155HG and ANXA2 were highly expressed in CRC tissues compared to non-cancerous tissues and the expressions of these two genes

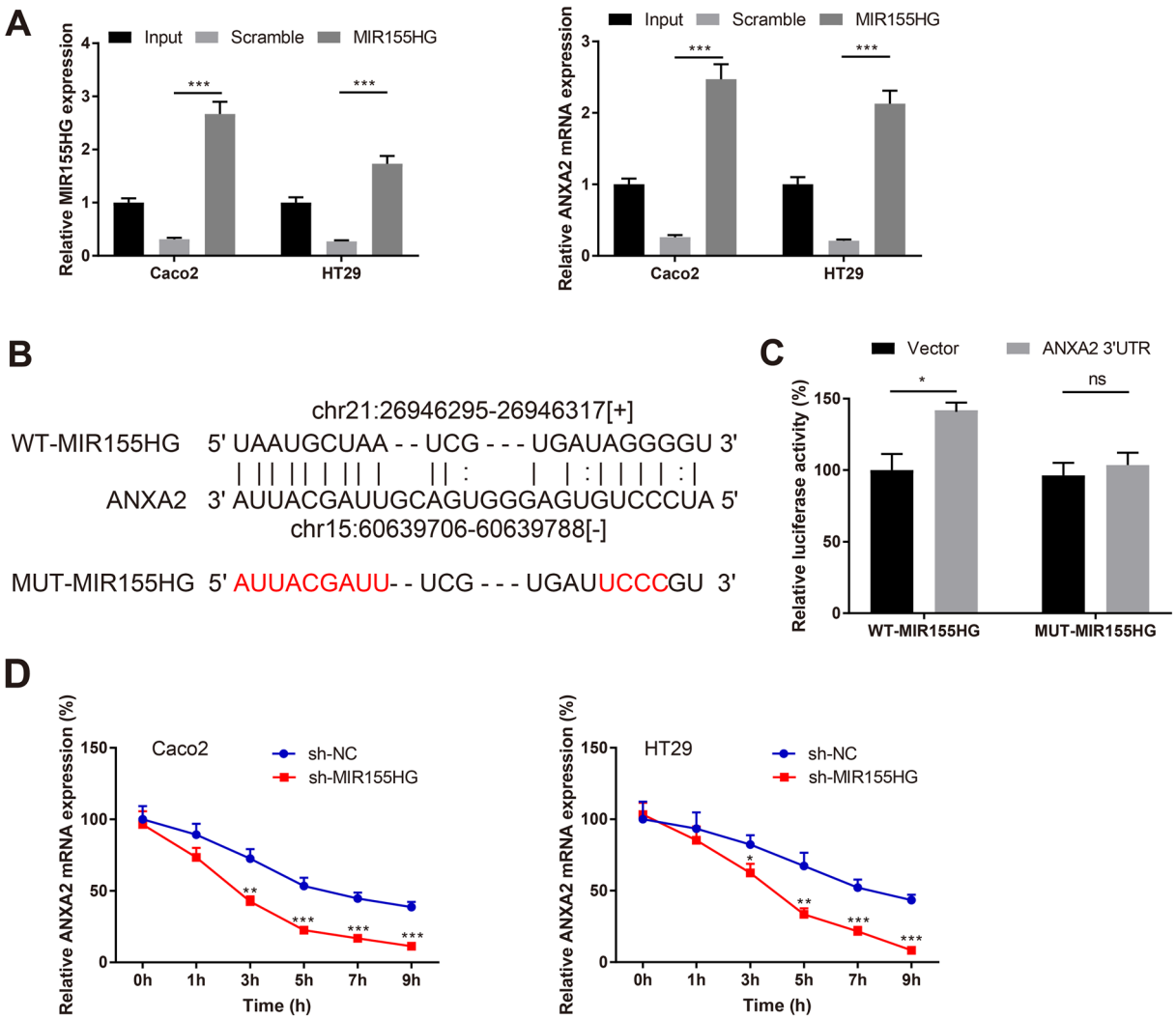

Fig. 6 LncRNA MIR155HG directly binds to and stabilizes ANXA2 mRNA. Notes: **a** RNA pull-down assay verified whether MIR155HG directly targeted ANXA2 in Caco2 and HT29 cells; **b** starBase predicted the binding site between MIR155HG and ANXA2 mRNA; **c** dual-luciferase reporter assay verified the binding site between MIR155HG and ANXA2 mRNA; **d** qRT-PCR detected the level of ANXA2 mRNA to determine the impact of MIR155HG knockdown on degradation rate of ANXA2 mRNA in Caco2 and HT29 cells. $^{*}P<0.05$, $^{**}P<0.01$, $^{***}P<0.001$

were positively correlated. Furthermore, overexpression of MIR155HG or ANXA2 predicted adverse pathological characteristics and poorer survival of CRC patients. Consistently, MIR155HG was dysregulated and seemed to be an unfavorable diagnostic marker in many malignancies, including natural killer/T-cell lymphoma [30], glioblastoma [31] and kidney renal clear cell carcinoma [32]. MIR155HG could promote mesenchymal transition in glioma and exert oncogenic effect by regulating miR-155-5p/-3p [33]. ANXA2 is an emerging biomarker for a variety of aggressive human cancers. Increased expression of ANXA2 is associated with invasion and metastasis in malignancies such as breast cancer [34], prostate cancer [35] and oral squamous cell carcinoma [36]. ANXA2 has been reported to promote proliferation and motility of CRC cells by remodeling motility relevant microstructures [37]. Moreover, ANXA2 could up-regulate STAT3 to enhance proliferation, invasion, and migration of CRC cells [38]. Consistent with the previous studies, MIR155HG and ANXA2 were highly expressed in CRC cell lines and knockdown of MIR155HG or ANXA2 suppressed the proliferation, migration and invasion of CRC cells.

Tissue-type plasminogen activator (tPA) recruited ANXA2 to induce phenotypic transformation of macrophages from M2 to M1 and thus resulted in increased renal inflammation [39]. In contrast, knockdown of MIR155HG or ANXA2 in CRC cells inhibited M2 polarization of macrophages, as demonstrated by reduction of CD206,

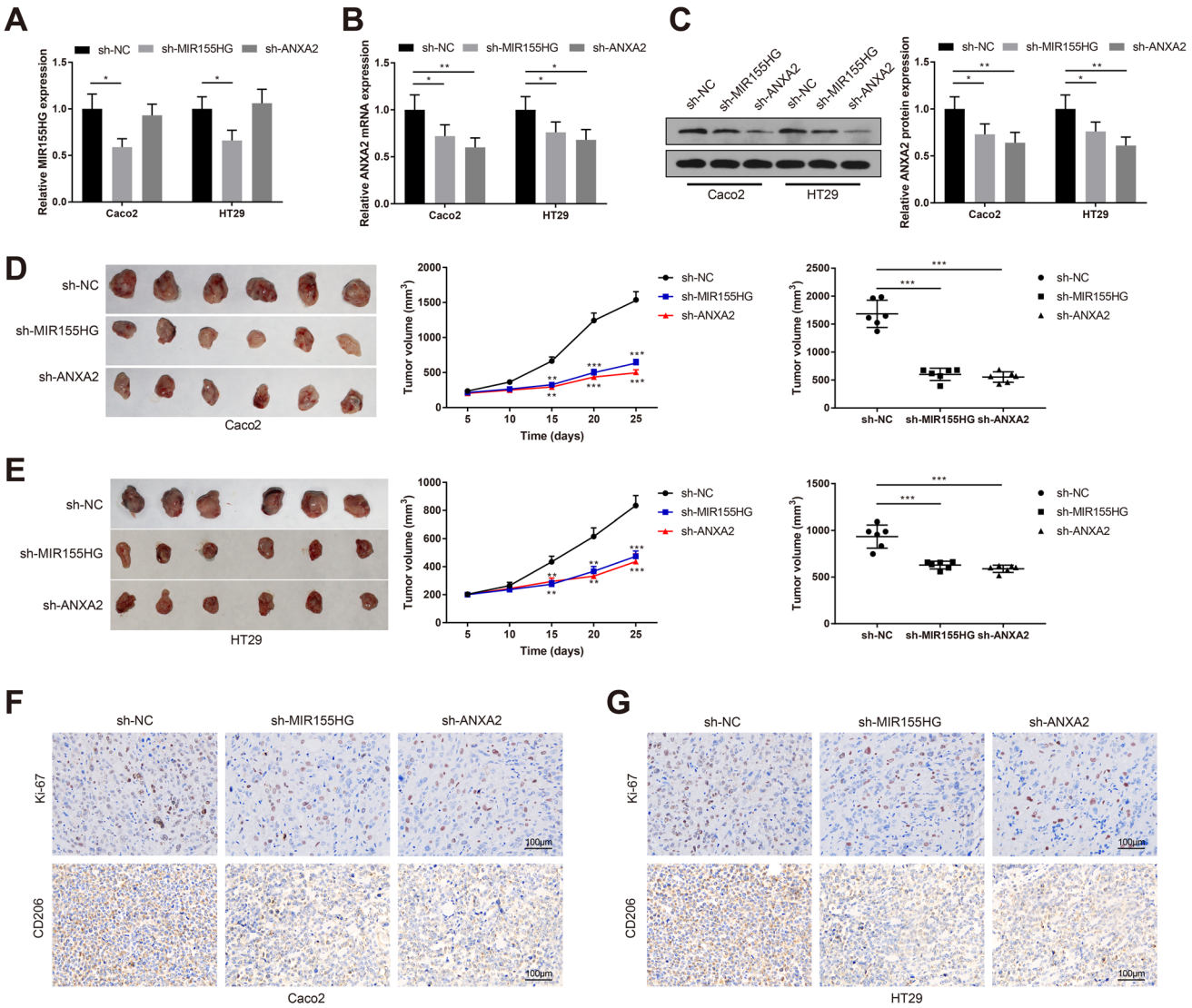

Fig. 7 Knockdown of lncRNA MIR155HG or ANXA2 inhibits CRC progression in nude mice. Notes: Heterotopic xenograft models of human CRC were established in nude mice. The expressions of MIR155HG (**a**) and ANXA2 (**b**–**c**) in tumors; **d**–**e** the effect of MIR155HG or ANXA2 knockdown on tumor size; **f**–**g** the effect of MIR155HG or ANXA2 knockdown on expressions of Ki-67 and CD206. $*P<0.05$, $**P<0.01$, $***P<0.001$; CRC, colorectal cancer

Arginase-1 and IL-10. M1 polarization was not affected by MIR155HG or ANXA2. M2 macrophage has been authenticated as a tumor promoter in many cancers. For instance, M2 macrophages promoted metastatic gastric and breast cancers by secreting CHI3L1 protein into tumor cells [40]. M2 macrophage-derived exosomes enhanced migration and invasion of CRC cells by delivering miRNAs [41]. Therefore, MIR155HG and ANXA2 might regulate the malignant behaviors of CRC cells by activating M2 macrophages. M2 macrophages have been reported to mediate sorafenib resistance in hepatocellular carcinoma by secreting hepatocyte growth factor [42]. We found that M2 macrophages could also modulate drug resistance of CRC cells. Knockdown of MIR155HG or ANXA2 increased the drug sensitivity of CRC cells by inhibiting M2 polarization. MIR155HG increased temozolomide resistance in glioma via the Wnt/β-catenin pathway [43]. ANXA2 can also protect tumor cells against chemotherapy in cancers like non-small cell lung cancer (NSCLC) [44] and bladder cancer [45]. Whether MIR155HG or ANXA2 regulates drug resistance in cancers via the assistance of M2 macrophages could be further studied.

The expressions of MIR155HG and ANXA2 were both down-regulated once MIR155HG was knocked down in CRC cells while ANXA2 inhibition did not affect the expression of MIR155HG. ANXA2 overexpression was found to reverse the suppression of MIR155HG knockdown on M2 macrophage polarization and cellular

activities of CRC cells, suggesting that MIR155HG might act on the progression of CRC by regulating ANXA2. Base on bioinformatics analysis, RIP assay and dual-luciferase reporter assay, miR-650 was detected to be a shared miRNA target of MIR155HG and ANXA2. Additionally, MIR155HG could directly target ANXA2 and stabilize ANXA2 mRNA. Since miR-650 is negatively regulated by MIR155HG in promoting CRC progression, miR-650 is supposed to be an oncogene in CRC herein. The suppressive role of miR-650 has been demonstrated before in the study conducted by Zhou et al. for analyzing the mechanism of miR-650 in non-metastatic CRC [46]. Also, miR-650 could suppress the development of glioma [47] and acute myeloid leukemia [48]. On the other hand, miR-650 has been identified as an oncogene in various cancers by mediating tumor cell proliferation, invasion and migration [49–51]. miR-650 displayed oncogenic effects in CRC cells by targeting inhibitor of growth protein 4 [52]. There seems no consensus about the effect of miR-650 on CRC progression and the role of miR-650 in CRC is waiting to be comprehensively explored in the future.

Finally, we demonstrated the promotive effects of MIR155HG and ANXA2 in heterotopic xenograft mouse models of CRC. Knockdown of MIR155HG or ANXA2 significantly reduced the tumor size of CRC mice. The proliferation of tumor cells and M2 macrophage polarization were also inhibited by MIR155HG or ANXA2 inhibition, evidenced by decreases in Ki-67 and CD206 positive cells.

In summary, MIR155HG promotes CRC progression and enhances drug resistance of CRC cells by mediating M2 macrophage polarization. MIR155HG plays its role in CRC via the miR-650/ANXA2 axis as well as by stabilizing ANXA2. MIR155HG is of significant prognostic value and may serve as a therapeutic target for aggressive CRC. As MIR155HG can also mediate drug resistance in CRC, MIR155HG-targeted therapy might improve the clinical outcomes of CRC patients.

At last, some limitations of this study must be mentioned. Subcutaneous xenograft transplantation is a widely used method to detect the effect of specific gene expression on tumor growth, and no significant toxicity has been reported. Nonetheless, this study does not provide data about vital organ toxicity since tissues and organs excepted for transplanted tumors were discarded after the mice were sacrificed. The expression of RNA would be affected in frozen tissues, which reduces the diagnostic value of biomarkers. Currently, there is no other available biological source for us to evaluate the efficacy of MIR155HG in CRC diagnosis. We expect to analyze the diagnostic value of MIR155HG from other biological source in our future study.

Supplementary Information The online version contains supplementary material available at https://doi.org/10.1007/s00262-021-03055-7.

Declarations

Conflict of interest The authors declare that they have no conflict of interest.

References

1. Siegel RL, Miller KD, Goding Sauer A, Fedewa SA, Butterly LF, Anderson JC, Cercek A, Smith RA, Jemal A (2020) Colorectal cancer statistics, 2020. CA Cancer J Clin 70:145–164. https://doi.org/10.3322/caac.21601
2. Arnold M, Sierra MS, Laversanne M, Soerjomataram I, Jemal A, Bray F (2017) Global patterns and trends in colorectal cancer incidence and mortality. Gut 66:683–691. https://doi.org/10.1136/gutjnl-2015-310912
3. Marmol I, Sanchez-de-Diego C, Pradilla Dieste A, Cerrada E, Rodriguez Yoldi MJ (2017) Colorectal carcinoma: a general overview and future perspectives in colorectal cancer. Int J Mol Sci. https://doi.org/10.3390/ijms18010197
4. Yamagishi H, Kuroda H, Imai Y, Hiraishi H (2016) Molecular pathogenesis of sporadic colorectal cancers. Chin J Cancer 35:4. https://doi.org/10.1186/s40880-015-0066-y
5. Chen J, Pitmon E, Wang K (2017) Microbiome, inflammation and colorectal cancer. Semin Immunol 32:43–53. https://doi.org/10.1016/j.smim.2017.09.006
6. Lasry A, Zinger A, Ben-Neriah Y (2016) Inflammatory networks underlying colorectal cancer. Nat Immunol 17:230–240. https://doi.org/10.1038/ni.3384
7. Shapouri-Moghaddam A, Mohammadian S, Vazini H et al (2018) Macrophage plasticity, polarization, and function in health and disease. J Cell Physiol 233:6425–6440. https://doi.org/10.1002/jcp.26429
8. Murray PJ (2017) Macrophage polarization. Annu Rev Physiol 79:541–566. https://doi.org/10.1146/annurev-physiol-022516-034339
9. Sica A, Larghi P, Mancino A et al (2008) Macrophage polarization in tumour progression. Semin Cancer Biol 18:349–355. https://doi.org/10.1016/j.semcancer.2008.03.004
10. Hao NB, Lu MH, Fan YH, Cao YL, Zhang ZR, Yang SM (2012) Macrophages in tumor microenvironments and the progression of tumors. Clin Dev Immunol 2012:948098. https://doi.org/10.1155/2012/948098
11. Li R, Zhou R, Wang H et al (2019) Gut microbiota-stimulated cathepsin K secretion mediates TLR4-dependent M2 macrophage polarization and promotes tumor metastasis in colorectal cancer. Cell Death Differ 26:2447–2463. https://doi.org/10.1038/s41418-019-0312-y
12. Shinohara H, Kuranaga Y, Kumazaki M, Sugito N, Yoshikawa Y, Takai T, Taniguchi K, Ito Y, Akao Y (2017) Regulated polarization of tumor-associated macrophages by miR-145 via colorectal cancer-derived extracellular vesicles. J Immunol 199:1505–1515. https://doi.org/10.4049/jimmunol.1700167
13. Yang C, He L, He P, Liu Y, Wang W, He Y, Du Y, Gao F (2015) Increased drug resistance in breast cancer by tumor-associated macrophages through IL-10/STAT3/bcl-2 signaling pathway. Med Oncol 32:352. https://doi.org/10.1007/s12032-014-0352-6
14. Zheng P, Chen L, Yuan X, Luo Q, Liu Y, Xie G, Ma Y, Shen L (2017) Exosomal transfer of tumor-associated macrophage-derived miR-21 confers cisplatin resistance in gastric cancer cells. J Exp Clin Cancer Res 36:53. https://doi.org/10.1186/s13046-017-0528-y
15. Beermann J, Piccoli MT, Viereck J, Thum T (2016) Non-coding RNAs in development and disease: background, mechanisms, and

therapeutic approaches. Physiol Rev 96:1297–1325. https://doi.org/10.1152/physrev.00041.2015
16. Ponting CP, Oliver PL, Reik W (2009) Evolution and functions of long noncoding RNAs. Cell 136:629–641. https://doi.org/10.1016/j.cell.2009.02.006
17. Zhang X, Wang W, Zhu W, Dong J, Cheng Y, Yin Z, Shen F (2019) Mechanisms and functions of long non-coding RNAs at multiple regulatory levels. Int J Mol Sci. https://doi.org/10.3390/ijms20225573
18. Yang X, Zhang S, He C et al (2020) METTL14 suppresses proliferation and metastasis of colorectal cancer by down-regulating oncogenic long non-coding RNA XIST. Mol Cancer 19:46. https://doi.org/10.1186/s12943-020-1146-4
19. Silva-Fisher JM, Dang HX, White NM et al (2020) Long non-coding RNA RAMS11 promotes metastatic colorectal cancer progression. Nat Commun 11:2156. https://doi.org/10.1038/s41467-020-15547-8
20. Zhang Y, Huang W, Yuan Y, Li J, Wu J, Yu J, He Y, Wei Z, Zhang C (2020) Long non-coding RNA H19 promotes colorectal cancer metastasis via binding to hnRNPA2B1. J Exp Clin Cancer Res 39:141. https://doi.org/10.1186/s13046-020-01619-6
21. Qin Y, Liu X, Pan L, Zhou R, Zhang X (2019) Long noncoding RNA MIR155HG facilitates pancreatic cancer progression through negative regulation of miR-802. J Cell Biochem 120:17926–17934. https://doi.org/10.1002/jcb.29060
22. Li N, Liu Y, Cai J (2019) LncRNA MIR155HG regulates M1/M2 macrophage polarization in chronic obstructive pulmonary disease. Biomed Pharmacother 117:109015. https://doi.org/10.1016/j.biopha.2019.109015
23. Thiele JA, Hosek P, Kralovcova E et al (2018) lncRNAs in non-malignant tissue have prognostic value in colorectal cancer. Int J Mol Sci. https://doi.org/10.3390/ijms19092672
24. Wu H, He G, Han H et al (2019) Analysis of MIR155HG variants and colorectal cancer susceptibility in Han Chinese population. Mol Genet Genomic Med 7:e778. https://doi.org/10.1002/mgg3.778
25. Chan JJ, Tay Y (2018) Noncoding RNA: RNA regulatory networks in cancer. Int J Mol Sci. https://doi.org/10.3390/ijms19051310
26. Wu W, Yu T, Wu Y, Tian W, Zhang J, Wang Y (2019) The miR155HG/miR-185/ANXA2 loop contributes to glioblastoma growth and progression. J Exp Clin Cancer Res 38:133. https://doi.org/10.1186/s13046-019-1132-0
27. Christensen MV, Hogdall CK, Jochumsen KM, Hogdall EVS (2018) Annexin A2 and cancer: a systematic review. Int J Oncol 52:5–18. https://doi.org/10.3892/ijo.2017.4197
28. Rocha MR, Barcellos-de-Souza P, Sousa-Squiavinato ACM, Fernandes PV, de Oliveira IM, Boroni M, Morgado-Diaz JA (2018) Annexin A2 overexpression associates with colorectal cancer invasiveness and TGF-ss induced epithelial mesenchymal transition via Src/ANXA2/STAT3. Sci Rep 8:11285. https://doi.org/10.1038/s41598-018-29703-0
29. Dekker E, Tanis PJ, Vleugels JLA, Kasi PM, Wallace MB (2019) Colorectal cancer. Lancet 394:1467–1480. https://doi.org/10.1016/S0140-6736(19)32319-0
30. Baytak E, Gong Q, Akman B, Yuan H, Chan WC, Kucuk C (2017) Whole transcriptome analysis reveals dysregulated oncogenic lncRNAs in natural killer/T-cell lymphoma and establishes MIR155HG as a target of PRDM1. Tumour Biol 39:1010428317701648. https://doi.org/10.1177/1010428317701648
31. Balasubramaniyan V, Bhat KP (2017) Targeting MIR155HG in glioma: a novel approach. Neuro Oncol 19:1152–1153. https://doi.org/10.1093/neuonc/nox095
32. Song J, Peng J, Zhu C, Bai G, Liu Y, Zhu J, Liu J (2018) Identification and validation of two novel prognostic lncRNAs in kidney renal clear cell carcinoma. Cell Physiol Biochem 48:2549–2562. https://doi.org/10.1159/000492699
33. Wu X, Wang Y, Yu T et al (2017) Blocking MIR155HG/miR-155 axis inhibits mesenchymal transition in glioma. Neuro Oncol 19:1195–1205. https://doi.org/10.1093/neuonc/nox017
34. Zhao C, Zheng S, Yan Z, Deng Z, Wang R, Zhang B (2020) CCL18 promotes the invasion and metastasis of breast cancer through Annexin A2. Oncol Rep 43:571–580. https://doi.org/10.3892/or.2019.7426
35. Yang N, Wang L, Liu J, Liu L, Huang J, Chen X, Luo Z (2018) MicroRNA-206 regulates the epithelial-mesenchymal transition and inhibits the invasion and metastasis of prostate cancer cells by targeting Annexin A2. Oncol Lett 15:8295–8302. https://doi.org/10.3892/ol.2018.8395
36. Liu XB, Wang J, Li K, Fan XN (2019) Sp1 promotes cell migration and invasion in oral squamous cell carcinoma by upregulating Annexin A2 transcription. Mol Cell Probes 46:101417. https://doi.org/10.1016/j.mcp.2019.06.007
37. He H, Xiao L, Cheng S et al (2019) Annexin A2 enhances the progression of colorectal cancer and hepatocarcinoma via cytoskeleton structural rearrangements. Microsc Microanal 25:950–960. https://doi.org/10.1017/S1431927619000679
38. Xiu D, Liu L, Qiao F, Yang H, Cui L, Liu G (2016) Annexin A2 coordinates STAT3 to regulate the invasion and migration of colorectal cancer cells in vitro. Gastroenterol Res Pract 2016:3521453. https://doi.org/10.1155/2016/3521453
39. Lin L, Hu K (2017) Tissue-type plasminogen activator modulates macrophage M2 to M1 phenotypic change through annexin A2-mediated NF-kappaB pathway. Oncotarget 8:88094–88103. https://doi.org/10.18632/oncotarget.21510
40. Chen Y, Zhang S, Wang Q, Zhang X (2017) Tumor-recruited M2 macrophages promote gastric and breast cancer metastasis via M2 macrophage-secreted CHI3L1 protein. J Hematol Oncol 10:36. https://doi.org/10.1186/s13045-017-0408-0
41. Lan J, Sun L, Xu F et al (2019) M2 macrophage-derived exosomes promote cell migration and invasion in colon cancer. Cancer Res 79:146–158. https://doi.org/10.1158/0008-5472.CAN-18-0014
42. Dong N, Shi X, Wang S et al (2019) M2 macrophages mediate sorafenib resistance by secreting HGF in a feed-forward manner in hepatocellular carcinoma. Br J Cancer 121:22–33. https://doi.org/10.1038/s41416-019-0482-x
43. He X, Sheng J, Yu W, Wang K, Zhu S, Liu Q (2020) LncRNA MIR155HG promotes temozolomide resistance by activating the Wnt/beta-catenin pathway via binding to PTBP1 in glioma. Cell Mol Neurobiol. https://doi.org/10.1007/s10571-020-00898-z
44. Feng X, Liu H, Zhang Z, Gu Y, Qiu H, He Z (2017) Annexin A2 contributes to cisplatin resistance by activation of JNK-p53 pathway in non-small cell lung cancer cells. J Exp Clin Cancer Res 36:123. https://doi.org/10.1186/s13046-017-0594-1
45. Hu H, Zhao J, Zhang M (2016) Expression of Annexin A2 and its correlation with drug resistance and recurrence of bladder cancer. Technol Cancer Res Treat 15:NP61–NP68. https://doi.org/10.1177/1533034615617078
46. Zhou C, Cui F, Li J, Wang D, Wei Y, Wu Y, Wang J, Zhu H, Wang S (2017) MiR-650 represses high-risk non-metastatic colorectal cancer progression via inhibition of AKT2/GSK3beta/E-cadherin pathway. Oncotarget 8:49534–49547. https://doi.org/10.18632/oncotarget.17743
47. Xu L, Yu QW, Fang SQ, Zheng YK, Qi JC (2018) MiR-650 inhibits the progression of glioma by targeting FAM83F. Eur Rev Med Pharmacol Sci 22:8391–8398. https://doi.org/10.26355/eurrev_201812_16537
48. Yuan C, Xu L, Du P, Pang J (2018) miRNA-650 exerts anti-leukemia activity by inhibiting cell proliferation through Gfi1 targeting. Tumori 104:369–374. https://doi.org/10.5301/tj.5000643

49. Qin A, Wu J, Zhai M, Lu Y, Huang B, Lu X, Jiang X, Qiao Z (2020) Axin1 inhibits proliferation, invasion, migration and EMT of hepatocellular carcinoma by targeting miR-650. Am J Transl Res 12:1114–1122
50. Tang X, Ding Y, Wang X, Wang X, Zhao L, Bi H (2019) miR-650 promotes non-small cell lung cancer cell proliferation and invasion by targeting ING4 through Wnt-1/beta-catenin pathway. Oncol Lett 18:4621–4628. https://doi.org/10.3892/ol.2019.10805
51. Zhao Y, Zhu Z, Shi S, Wang J, Li N (2019) Long non-coding RNA MEG3 regulates migration and invasion of lung cancer stem cells via miR-650/SLC34A2 axis. Biomed Pharmacother 120:109457. https://doi.org/10.1016/j.biopha.2019.109457
52. You Q, Li H, Liu Y et al (2018) MicroRNA-650 targets inhibitor of growth 4 to promote colorectal cancer progression via mitogen activated protein kinase signaling. Oncol Lett 16:2326–2334. https://doi.org/10.3892/ol.2018.8910